SSRG International Journal of Mechanical Engineering
ISSN: 2348-8360/ https://doi.org/10.14445/23488360/IJME-V12I9P102

Volume 12 Issue 9, 15-28, September 2025

Original Article

Performance Analysis and Optimization of Undershot Water Wheel for Small-Scale Hydropower Applications

Prashanth Kumar Sanjeevaiah[1,2], Ramesh Kumar Donga[1], Ashish Karn[1]

[1]*Department of Mechanical Engineering, School of Advanced Engineering, UPES, Dehradun, India.*
[2]*Department of Mechanical Engineering, Sheshadripuram Institute of Technology, Karnataka, India.*

[1]*Corresponding Author : 500095530@stu.upes.ac.in*

Received: 03 July 2025 Revised: 04 August 2025 Accepted: 05 September 2025 Published: 30 September 2025

Abstract *- This study examines the performance of four undershot water wheels with different blade counts and profiles to identify the optimal setup for small-scale hydropower. The original wheel (nO24), with 24 flat blades and installed at the Kalinga canal in Dehradun, India, is compared to new (N) designs with 24 (nN24), 36 (nN36), and 48 (nN48) curved blades. All models have a 1-meter diameter, scaled down at a 4:1 ratio and tested in the turbine facility at the UPES Fluid Mechanics Lab, Dehradun. Design Expert 13 (DoE) software was used to optimize the number of experiments. Tests were conducted under varying flow rates, heads, and loads to evaluate hydraulic efficiency (η) and mechanical power (P). The nO24 wheel failed at higher loads (1.85 L/s), while the nN24 reached a maximum efficiency of 58%, improving by 6% over nO24. The nN36 outperformed all, achieving 65% efficiency and 1.35 W power output. In comparison, nN48 had reduced productivity from flow interference. Overall, nN36 had the highest efficiency-power trade-off with an increased power output of 27%. This study has shown that curved blade designs, in general, could be beneficial for undershot wheels used in decentralized, small-scale hydropower systems.*

Keywords *- Micro water turbine, Water wheel, Turbine blades, Power, Efficiency, Response surface method.*

1. Introduction

Small-scale hydropower acts as an effective pathway towards a decentralized and sustainable source of electricity, especially in rural and remote areas with little or no access to conventional sources of energy [1, 2]. In this arena, undershot water wheels have gained renewed interest in producing electricity in shallow rivers and ultra-low head situations since they do not necessitate dams or major civil works [3, 4]. Their low-cost, simple construction and relatively low ecological impact make them prime candidates for small-scale renewable energy systems [5, 6].

Traditionally, undershot wheels were supplanted by overshot wheels and modern turbines, which provide higher efficiencies and broader operating conditions. Overshot wheels often operate above 80% efficiency, while undershot wheels at best often work in the 65–75% efficiency range [7-9]. Not only do turbines like the propeller and crossflow designs enhance efficiency, but they also enhance operational reliability and even lower the reliance on traditional undershot wheels in the mainstream hydropower sector [10, 11]. Nonetheless, undershot wheels have re-emerged as reliable forms of eco-friendly and decentralized energy in rural electrification and water-lifting applications; when turbines can be impractical or economically burdensome, undershot wheels can provide a source of energy in rural areas [12].

The performance of undershot wheels is sensitive to design parameters such as blade geometry, blade count, immersion depth, and flow rate. Flat blades are an easy structural option, but they are not efficient [13] compared to curved or bowl-shaped blades, which improve hydrodynamic energy capture [14, 15]. Similarly, blade counts affect torque and efficiency; however, too many blades can lead to turbulence that may negatively affect the performance [16, 17] Computational Fluid Dynamics (CFD) studies have rendered useful insight into these parameters, [18, 19] yet the predicted performance is subject to assumptions dealing with turbulence, boundary conditions, and geometric simplifications, making experiments even more necessary [20].

While these developments are promising, most previous studies examined either blade shape or blade count independently with little experimental verification under controlled hydraulic conditions. There are not many systematic studies that consider blade shape and blade count together, which creates uncertainty on how to best optimize an undershot wheel for practical low-head applications.

The present study fills this gap through a series of controlled flume experiments that directly compare the original bi-folded 24-blade wheel (nO24) with a curved-blade wheel with newly developed shapes with 24 (nN24), 36 (nN36) and 48 (nN48) blades. By systematically studying the efficiency, torque and adaptability of the wheels across a range of flow rates and applied loads, this work presents new, experimentally-validated knowledge on the combined effects of shape and blade count on the performance of an undershot wheel, which provides direct specifications for developing cost-effective and sustainable micro-hydro systems.

2. Literature Review

Undershot water wheels are well-established for their simplicity and suitability to low-head applications (generally 0.3-1.5 m) [21]. Historical examples of the Zuppinger and Sagebien wheels had the ability to efficiently operate at ultra-low head. These prior models, such as in an early example of a Zuppinger wheel from the 1850s, have efficiencies for ultra-low-head sites, where retrofitting possibilities are at either new non-powered weirs or mills of head (H_w) of up to 2.5 m is an added benefit. Water wheels have also been adapted more recently through modifying with other technologies where wheels operating at moderate head ranges from as low as 0.5 m and a moderate "high-head" of just under nearly 12 m [22]. While water wheels have played an important historical role, undershot wheels are less popular than their overshot wheel counterparts and turbine systems, which typically achieve higher efficiencies and broader energy ranges under varying conditions [23].

In general, flat blades have not shown good performance; Nguyen et al. (2018) observed very low efficiencies (<40%) in both their experimental and modelling results with flat blades [13]. Quaranta & Revelli (2017) showed a small improvement in efficiency (4–5%) using curved blades, which was likely due to the interaction between the wheel and the water being smoother, less turbulent, and better capturing the hydrodynamic characteristics of the water and blade shapes [14, 24]. Blade number has also been an important consideration: Permanasari et al. (2019) found blade number to be the largest impact factor in their model (68.1%), followed by blade shape and then flow rate [16]. The study indicated that holding too many blades (>48 blades) caused more drag, which is detrimental to the long-term efficiency of the water wheel [25]. In addition, immersion depth does impact energy capture because submersion depth needs to maximize impact force while minimizing drag [26]. Experimental approaches have shown mixed results for blades that were angled or bi-fold blade designs. The efficiencies of designs have varied significantly, ranging from below 15 % for wheels with 12-curved blades [27] to ~33 % with certain bi-fold designs [28].

Computational Fluid Dynamics (CFD) has transformed undershot wheel design, enabling research to optimize blade shapes and configurations for performance [29, 30]. The performance increases found from CFD studies for curved blades (approximately 4% increased performance) compared to flat or elliptical blades are outweighed by experimental verification of bowl-shaped blades achieving efficiencies of over 70% under appropriate test conditions [15]. However, the continued limitations to hydrokinetic turbine research are in the simplified turbulence models, unrealistic boundary conditions and approximations of geometry, and the high computational costs associated with high-fidelity models (and thus the need for experimental verification). As in hydrodynamic research, the assumptions made in numerical models can be drastically different from those in real hydraulic environments. Particle Image Velocimetry (PIV) and experimental studies provide complete information that overlaps with the investigation of real flow environments around blades, and ensure that CFD predictions are aligned with real conditions [17].

Undershot wheels are increasingly used for rural electrification because they are inexpensive and easy to construct, which means these systems can be deployed in communities where resources are scarce [31]. In Indonesia, successful undershot wheels have been used to supply electricity to remote villages. These systems can also be used for irrigation by integrating with spiral tube pumps, which simultaneously lift water while generating power [32, 33].

The economic feasibility of undershot wheels provides an even more compelling reason for their importance. They are a low-cost option for energy generation in rural and remote areas where there are limited options for electricity [34]. Undershot wheels often incur only 33-66% of the capital costs of turbine technologies [14, 24] and have payback periods of 7 to 14 years based on flow conditions.

Their relatively low-cost systems can even be installed on a community or individual scale [35-37], and they provide local job opportunities for manufacturing parts, mechanical installations, and general maintenance [38]. Existing models like the Zuppinger wheel illustrate how one can take advantage of proven finalized designs and provide rigorous and innovative cost-effective retrofits within the reconversion of old mills and weirs.

The ecological studies also exhibit the benefits of undershot wheels. Compared with turbines, undershot wheels operate within a smaller ecological footprint, maintain river morphology and flow, and allow easier and more effective fish passage [39, 40]. Undershot wheels can provide other multifunctional benefits, such as using a spiral tube pump with an undershot wheel to provide agricultural irrigation and electrical power at the same time [32, 33]. The environmental acceptability, potential for job creation, and applicability for rural electrification have raised the profile of undershot wheels in sustainable hydropower interventions [41].

Another important gap is the long-term performance of undershot wheels, specifically with regard to wear and durability and sustained operation. The scale-up of findings from the lab to the field prototype scales introduces uncertainty as the Reynolds number and Froude similarity introduce distortions to torque and efficiency [42]. Although research into turbine blade design has explicitly identified geometry and arrangement as important determinants for efficiency, there has yet to be a quasi-systematic cross-comparison of undershot blade designs undertaken in the intended conditions of loading and flows.

This knowledge gap has highlighted the importance of this experimental study that systematically studies undershot wheels with various blade geometries (bi-fold and curved) and numbers of blades (24, 36, and 48). By bringing together controlled flume tests and performance assessments of flows and applied loads, this study will add important validated data on torque, efficiency, and performance to previous data in the literature.

The methodology provided in the following section outlines the experimental setup and testing procedures set out to allow a better understanding of undershot wheel optimization to be more competitive with low-head hydropower applications.

3. Materials and Methods

This section provides a comprehensive overview of the experimental setup, including the design process for various water wheels and their testing under controlled conditions. Detailed descriptions of fabrication techniques, experimental procedures, and performance analysis are presented.

3.1. Blade Design

Four undershot water wheel models were tested in this study. The reference model (nO24) is an undershot water wheel with 24 bi-fold blades, scaled down from a prototype wheel installed in the Kalinga Canal, Dehradun, India. Using the geometric similarity, the reference undershot water wheel is scaled down with a scale ratio of 4.

Three newly designed wheels (nN24, nN36, nN48) with curved blades were fabricated to investigate the effect of blade geometry and blade count on performance. The blade curvature was defined using a wheel-to-blade radius ratio (R/r) of 4 [43]. Figure 1 (a) shows an undershot water wheel with 24 bi-fold blades having a radius of 2 meters and a blade width of 1.2 meters.

Figure 1 (b) shows the 3-D design of the nO24 water wheel used for 3-D prototyping, and Figure 1 (c) shows the 3-D printed and assembled model of the nO24 water wheel. The specifications of the water wheel with curved blades and hydraulic flume experimental setup are shown in Table 1.

(a)

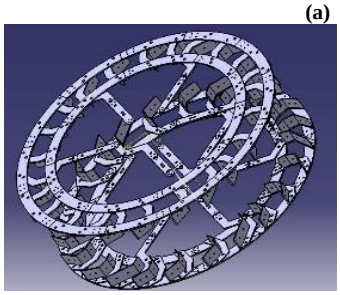

(b)

(c)

Fig. 1 (a) Existing water wheel with 4 m diameter and 24 blades, (b) 3-D design with scale ratio 4 for 3-D prototyping, and (c) 3-D model of the existing water wheel with scale ratio 4.

Table 1. Specifications of undershot water wheels and hydraulic flume experimental setup

Parameters	Symbol	Value	Units
Undershot Water Wheel Design			
External diameter	D_e	1000	mm
Blade width	W	300	mm
Blade curvature diameter	d	250	mm
Water inlet angle	α	116	degrees
Blade length	l	506	mm
Water inlet angle	θ	150	degrees
Shaft diameter	d_s	40	mm
Torque collar thickness	t	7	mm
Clearance from the bed	C	10	mm
Number of blades	N	24, 36, 48	no.
Spacing between blades	N24, N36, N48	15, 10, 7.5	degrees
Hydraulic Flume Specifications			
Flume channel dimensions	(l × w × d)	10 × 0.6 × 0.75	m^3

Flume reservoir dimensions	(l × w × h)	1.5 × 1.1 × 1.35	m^3
Centrifugal pump motor power	HP	10 (7.5)	kW
Pump inlet diameter		0.15	m
Pump outlet diameter		0.15	m
Orifice diameter		0.09	m

3.2. Fabrication, Assembly, and Installation of the Water Wheels

The fabrication of the models was carried out using a combination of 3-D printing and thermoforming. The individual wheel components were first modeled in CATIA and then processed in PrusaSlicer software to generate G-code with a slicing resolution of 0.2 mm. Figure 2 (a) and Figure 2 (b) show the 3-D Models arranged on the Prusa slicer software bed and sliced images of the 3d models for G-code generation, respectively.

The components were fabricated using a Creality CR-M4 3-D printer with a 450 × 450 mm bed size, employing PLA filament at 40% infill density to balance strength and weight. This approach ensured dimensional accuracy and reduced overall weight, making the wheels suitable for testing in the laboratory flume. The curved blades were produced separately from acrylic sheets using thermal forming with a die and mould, and were subsequently assembled with the 3-D printed hubs, holders, and support rods.

The adoption of 3-D printing allowed precise blade positioning and reduced both the cost and fabrication time compared to conventional sheet-metal manufacturing. Figures 2 (c) and (d) show the 3-D printing of the bi-fold blade holder and supporting structure rods used in the nO24 wheel.

3-D printing reduces the cost and time required to fabricate the wheel while ensuring it stays light enough for testing with the available flow rate in the flume. Figure 3 shows the 3-D design and 3-D printed water wheel models with curved blades, which have 24, 36, and 48 blades assembled and installed in a flume for testing.

(a)

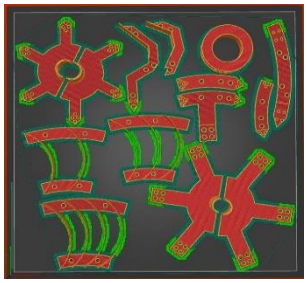

(b)

(c)

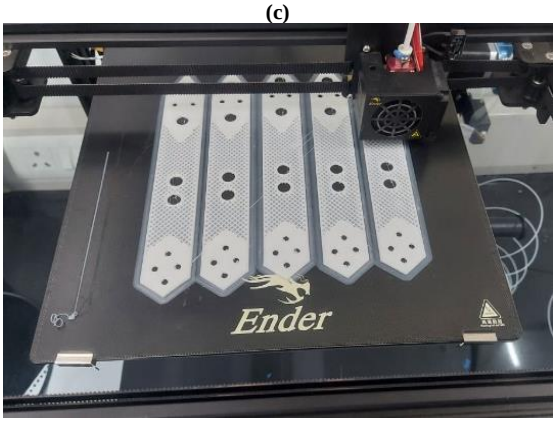

(d)

Fig. 2 3-D models and printing of experimental setup (a) Arranged on Prusa slicer software bed, (b) Sliced for G-code generation, (c) bi-fold blade holder, and (d) supporting structure rods used in the nO24 wheel.

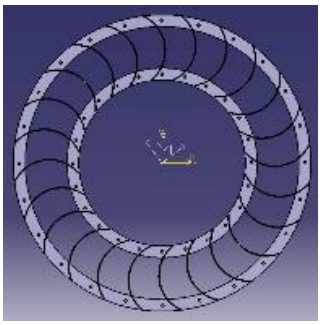

(a)

(d)

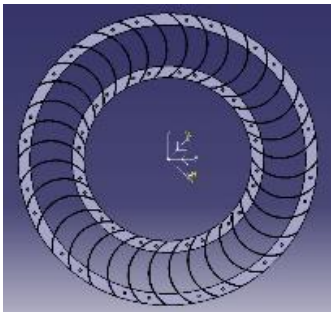

(b)

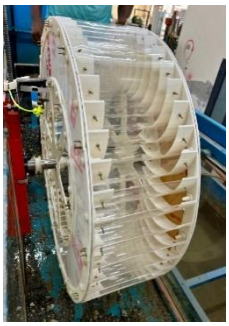

(e)

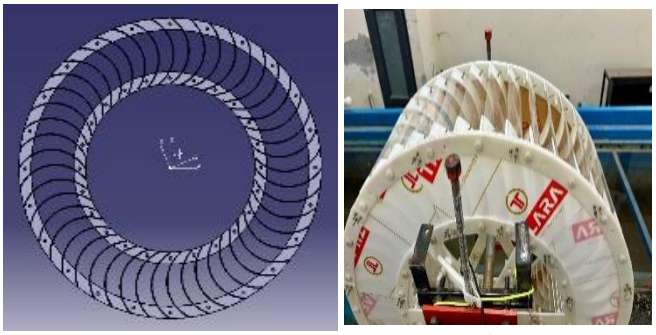

(c) (f)

Fig. 3 (a), (b) and (c) 3-D design of water wheels used for prototyping, (d), (e) and (f) 3-D printed and assembled water wheels in the flume for testing. (a) & (d) 24 (nN24), (b) & (e) 36 (nN36) and (c) & (f) 48 (nN48) curved blades water wheels

3.3. Experimental Setup

The experimental tests were conducted in a recirculating hydraulic flume installed in the Fluid Mechanics Laboratory at UPES, Dehradun. The flume measured 10 m in length, 0.6 m in width, and 0.75 m in depth, and was supplied by a centrifugal pump driven by a 10 HP (7.5 kW) motor through 150 mm suction and delivery pipes connected to a rectangular reservoir tank measuring 1.1 m in width, 1.5 m in length, and 1.35 m in height Figure 4 (a). The wheel was mounted on a 40 mm diameter galvanized iron shaft, supported by bearings in take-up frames that allowed vertical adjustment. The assembly was installed 7 m downstream from the flume inlet, ensuring that water flow stabilized before reaching the wheel. Flow regulation was achieved using a control valve in combination with an orifice meter and a U-tube manometer, Figures 4 (b) and (c). Flow velocity was also measured independently using a pygmy-type current meter connected to a velocity logger, Figures 4 (d) and (f).

Torque and load measurements were obtained using a brake-drum dynamometer-like setup. One end of a rope wound around the torque collar was tightened with a threaded nut, while the opposite end was connected to a load cell with a maximum capacity of 10 kg, Figure 4 (e). The rotational speed of the wheel was measured using an infrared sensor that recorded binary RPM data at one-second intervals, based on the reflection of light from tape attached to the shaft. All 3-D printed parts were inspected and finished prior to assembly to ensure dimensional accuracy and smooth operation during experiments.

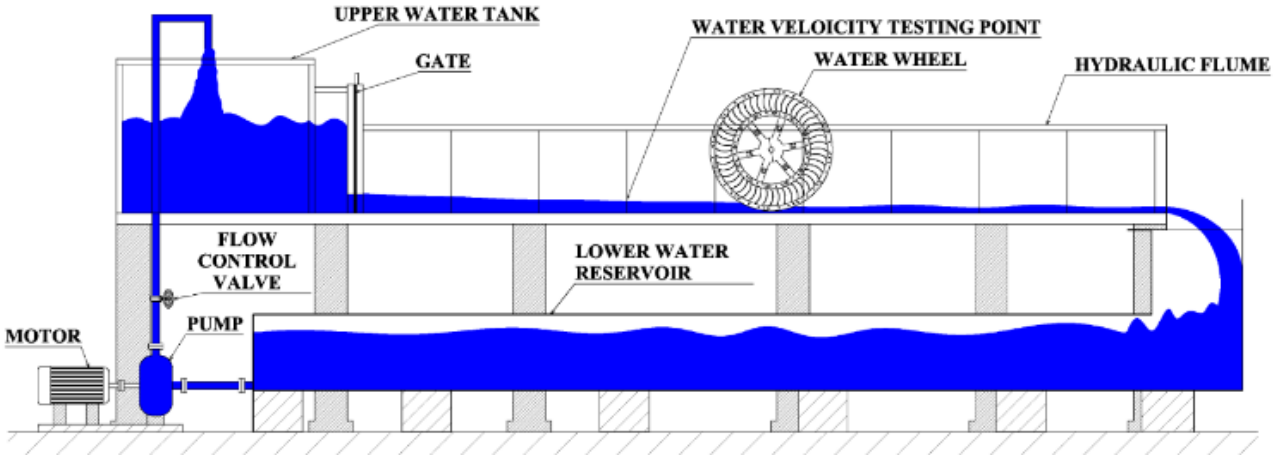

(a)

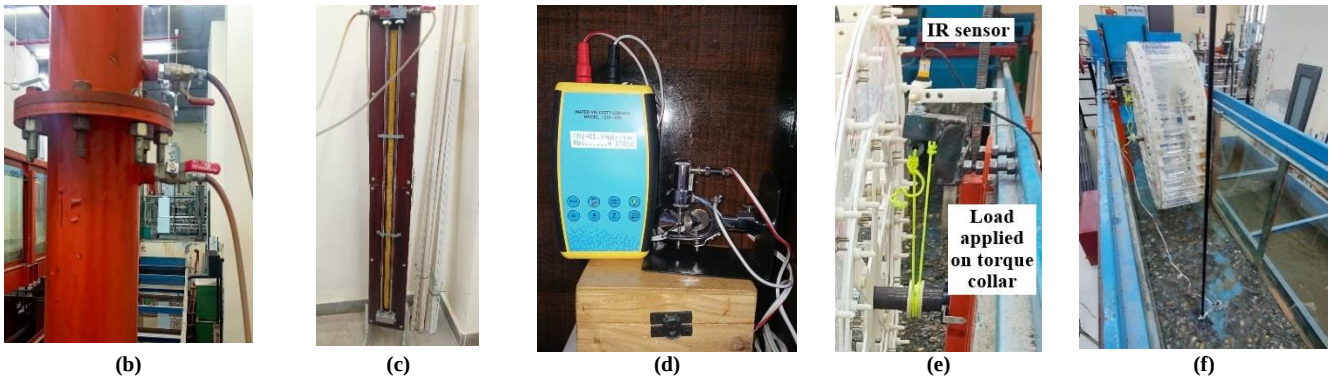

(b) (c) (d) (e) (f)

Fig. 4 Water wheel assembly installation in the lab within the hydraulic flume (a) Schematic diagram of the experimental setup, (b) Orifice installed in the pipeline, (c) U-tube manometer connected to the pipeline, (d) Pygmy-type water current meter, (e) load applying setup, and (f) Current meter in the flume recording the velocity of water.

The experiments were designed using the Central Composite Design (CCD) approach in order to capture the effects of two major factors, such as flow rate and applied load, on wheel performance. Flow conditions were varied by adjusting the manometer head to 2 cm, 4 cm, and 6 cm, while the applied load was systematically altered using the brake-drum system.

The measured response variables included torque, power output, rotational speed, and efficiency. The use of CCD allowed efficient coverage of the design space and the evaluation of nonlinear interactions between flow rate and load while reducing the total number of trials compared to a full factorial design.

3.4. Uncertainty Analysis

An uncertainty analysis was conducted in this study to evaluate the accuracy of the measured parameters, given the experimental nature of the research and the use of various measurement instruments. Device errors were determined, and uncertainties in dependent variables were computed using the error propagation method. The combined uncertainty was calculated by taking the root of the sum of the squares of individual errors.

The maximum uncertainties observed for hydraulic power, shaft power, and efficiency were ±0.97%, ±0.73%, and ±0.65%, respectively. At an applied load of 4.5 kg and a discharge of 1.85 L/s, the highest efficiency uncertainty of ±0.65% was noted, with a total efficiency uncertainty across experimental trials calculated at ±2.97%. Measurement errors included a manometer resolution error of 0.0005 m, a measurement deviation of 0.003 m, and a calibration error of 0.0002 m.

The head values were measured at depths of 0.272 m, 0.544 m, and 0.816 m of water, corresponding to the manometer readings of 2 cm Hg, 4 cm Hg, and 6 cm Hg. The orifice diameter error was 0.09 m, while the coefficient of Discharge (C_d) was constant at 0.67. Gravitational acceleration (g) was assumed to be 9.81 m/s². Scale resolution errors for clearance measurements were 0.0005 m. The pygmy-type current meter recorded a flow rate uncertainty of 0.003183 m³/s, and the load cell accuracy error was ±0.05%.

3.5. Data Analysis

The experimental data were systematically analyzed to compute key performance parameters, including the undershot water wheels' Discharge, hydraulic, and shaft power. Measurements from flow meters, manometers, and load cells were processed to evaluate the energy transfer efficiency under varying flow rates and loading conditions.

3.5.1. Discharge in the Flume

The differential head (x) measured using the manometer determines the water discharge in the flume. The manometer is filled with mercury. Thus, the differential head (H_w) measured using a manometer is converted into water head using Equation (1) and the flume discharge is measured using Equation (2) [44].

$$H_w = x\left(\frac{\rho_{Hg}}{\rho_{H_2o}} - 1\right) \quad (1)$$

$$Q = C_d * \frac{a_1 a_o}{\sqrt{a_1^2 - a_o^2}} * \sqrt{2 * g * H_w} \quad (2)$$

$$a = \frac{\pi * d^2}{4} \quad (3)$$

Where C_d is the coefficient of Discharge of the orifice (0.67), $a_o and\ a_1$ are the pipe and orifice area computed using the diameter of the pipe (d_p =150mm) and orifice diameter (d_o = 90mm), respectively, g is the acceleration due to gravity (9.81 m/s^2), ρ_{Hg} is the density of the mercury (13600 kg/m^3), and ρ_{H2O} is the density of the water (1000 kg/m^3).

3.5.2. Discharge and Hydraulic Power (P_h) Available to the Wheel

The flume used in this study has a width (W) of 0.6 m. The water wheel was designed using model analysis with a scale ratio of 4, resulting in a scaled-down model with a width (W_b) of 0.3 m.

The corresponding full-scale prototype has a wheel width (W_p) of 1.2 m. Thus, the hydraulic power available to the wheel results from the water acting on the wheel, not the flume discharge. The Discharge acting on the blades is determined by calculating the water depth to the free surface level using the continuity Equation (6) [45].

$$Q = A * V \quad (4)$$

$$Q = W * D * V \quad (5)$$

$$D = \frac{Q}{W * V} \quad (6)$$

The hydraulic power acting on the wheel is due to the fluid's kinetic energy impacting the blades. As it depends on the immersion depth of the blade, the blade area used in Equation (7) is computed by subtracting the clearance (C) of the wheel from the flume bottom to the free surface of water or water depth in the flume.

$$A_b = (D - C) * W_b \quad (7)$$

The blade area (A_b) and the water velocity in the flume (V) are used to calculate the hydraulic power available to the wheel, as shown in Equation (8) (Nishi et al., 2016). A water current meter measures the water velocity (V). Three velocities used in the study produce varied depths of

immersion, resulting in three hydraulic powers available to the wheel [23].

$$P_h = \frac{1}{2}\,\rho\, A_b\, V^3 \tag{8}$$

Where, Q is the water discharge (m^3/s), A is the pipe area (m^2), V is the water velocity (m/s), W is the width of the channel (m), D is the depth of the water from the free surface level in the channel (m), C is the clearance between the flume floor to the blade tip (m), W_b is the blade width (m), A_b blade area immersed in water (m^2) and P_h is the hydraulic power available to the water wheel (W).

3.5.3. Shaft Power (P_s)

A torque collar mounted on the shaft and the rope wound around it is used to apply a load on the wheel by connecting one end of the rope to the nut, which increases tension in the rope upon tightening. And the other end of the rope is connected to the load cell, which records the load applied (L) for the trial period of 5 minutes with a period of 1 second. The average applied load is considered to compute the force acting on the torque collar. The effective radius of the shaft is the combination of the shaft radius (r_s) and the thickness of the torque collar (t). The applied torque acting on the wheel is computed using Equation (9).

$$T = L * g * (r_s + t) \tag{9}$$

Using the IR sensor, the wheel's rotation is measured as binary. The value recorded for 5 minutes was averaged over 1 minute to calculate the RPM. The shaft power is then calculated for each trial using Equation (10) [46].

$$P_s = \frac{2\,\pi\, N\, T}{60} \tag{10}$$

$$\eta_w = \frac{P_s}{P_h} \tag{11}$$

Where L is the load applied on the wheel (kg), r_s is the radius of the shaft (m), t is the thickness of the torque collar (m), N is the RPM measured using an IR sensor, T is the torque applied on the wheel (N-m), and η_w is the efficiency of the water wheel.

3.6. Data Processing

Figure 5 illustrates the data collection system implemented for this study. The study employed a 10 kg load sensor/load cell that outputs an electrical signal in millivolts. Moreover, the output signal is amplified via a signal amplifier (HX711) to the 5-volt input required by the Arduino Uno for the data processing. The IR sensor (E18 D80NK) is also wired to the Arduino Uno to output the 5 volts needed for data processing. The input signals to the Arduino board come from the load cell signal amplifier and the IR sensor, which the Arduino board processes using the C programming language.

The C program was modified to fulfil two functions: (a) calibrating the load cell, and (b) collecting load and IR sensing data from the Arduino Uno at a time interval of 1 second. The load cell was calibrated at the start of every trial with the physical 2 kg weight. The data acquired was saved in a .txt file for each trial at 1-second intervals, which enables 300 total readings for each trial. The data is further analyzed in MATLAB to calculate hydraulic power (P_h), shaft power (P_s), and the efficiency (η) of the water wheel. Further, MATLAB is used to plot the performance curves such as shaft power (P_s) vs RPM (N), torque (T) vs RPM (N), and efficiency (η) vs RPM (N).

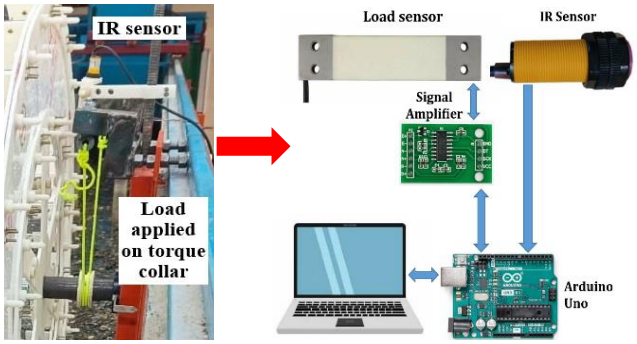

Fig. 5 Data collection and processing setup integrated with the setup

3.7. Experimental Design and Statistical Analysis

The experiments for each water wheel were designed using the Central Composite Design (CCD) method implemented in Design Expert 13 software. The factor ranges were selected based on the functional limits of the measuring instruments and controlled manipulation of operating conditions to ensure accuracy. Flow rates were determined using a manometer connected to an orifice meter, with differential heads of 2 cm, 4 cm, and 6 cm, corresponding to discharges of 1.85 L/s, 2.88 L/s, and 3.88 L/s, respectively. The applied loads were set with a 10 kg load cell at three levels: 0 kg, 4.5 kg, and 9 kg. Three blade configurations were tested: 24 blades (15° spacing), 36 blades (10° spacing), and 48 blades (7.5° spacing).

Each wheel underwent 13 trials. Trials 1–3 were performed without load at manometer heads of 2 cm, 4 cm, and 6 cm. Trials 4–10 were carried out with a 4.5 kg load across the same three head levels, with additional repetitions at 4 cm to establish baseline stability. Trials 11–13 were conducted with a 9 kg load at 2 cm, 4 cm, and 6 cm head levels. This systematic test plan ensured all factor combinations were captured within a structured and controlled design matrix. The CCD framework enabled evaluation of both individual and interactive effects of blade count, flow rate, and applied load on performance parameters such as power output and efficiency. Statistical analysis was performed using Analysis of Variance (ANOVA) in Design Expert 13 to identify the significance of main effects and interactions.

The quality of the predictive models was evaluated using the coefficient of determination (R^2). An R^2 value close to 1 indicates that the model explains nearly all of the observed variability in the experimental data, reflecting a strong agreement between predicted and measured values. Thus, high R^2 values confirmed the robustness of the developed models in capturing the influence of operating and design parameters on water wheel performance.

4. Results and Discussion

This section evaluates the performance of the water wheels with original (O) design and blades nO24, and new design (N) and blades nN24, nN36, and nN48 under flow rates of 1.85 L/s, 2.88 L/s, and 3.88 L/s produced at differential heads of 2cm, 4cm, and 6cm respectively and tested across three loading conditions 0 kg, 4.5 kg, and 9 kg. The analysis focuses on two critical output parameters: hydraulic efficiency (η) and mechanical power (P).

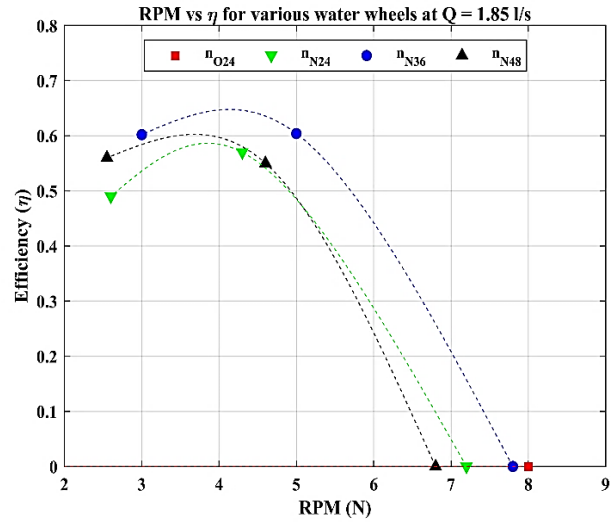

(a)

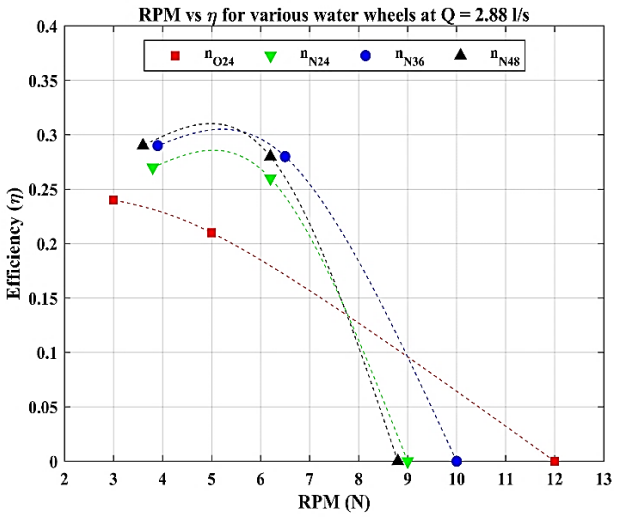

(b)

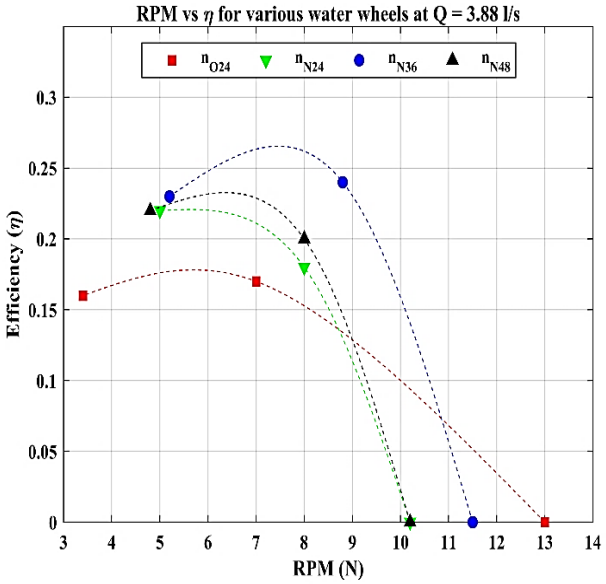

(c)

Fig. 6 Effect of blade design and count on efficiency for varied flow rates of (a) Q= 1.851 l/s, (b) Q= 2.88 l/s and (c) Q= 3.88 l/s undershot water wheel

Figure 6 shows the change in the efficiency of the different water wheels at varied wheel speeds due to applied load and three flow rates: 1.85 l/s, 2.88 L/s, and 3.88 L/s. The effect of the blade geometry is observed in all the flow rates, where at 1.85 L/s, the nO24 water wheel has stopped working as the load increases, showcasing its inability to handle moderate to heavy loads compared to nN24, which easily produces maximum efficiency up to 58% at 3.9 RPM.

This response of the nO24 water wheel is attributed to the blade geometry, and backlash resulted due to the inaccurate blade distribution on the wheel. At 2.88L/s and 3.88 l/s, despite the nO24 exhibiting improvement in efficiency, the nN24 outperformed nO24 significantly. The maximum efficiency of nN24 is improved by up to 6% compared to nO24 at 2.88 L/s, producing 5 RPM, and 5% at 3.88 L/s, producing 5.5 RPM. This indicates that undershot water wheels' curved blades are more efficient than flat or bi-fold blade designs.

Comparing the water wheel with different blade counts, 24 (nN24), 36 (nN36), and 48 (nN48), the nN36 has exhibited maximum efficiency at 1.85 L/s (65%) and 3.88 L/s (27%) water flow rates. Meanwhile, the nN48 exhibits higher efficiency (31%), which is very close to nN36 (30.5%), at moderate flow rates of 2.88 L/s. This behavior of the nN48 wheel indicates that the increased blade count after 36 blades results in increased blockage to the water flow due to the narrow spacing between the blades. This leads to insufficient time for energy transfer interaction between the blade and the water.

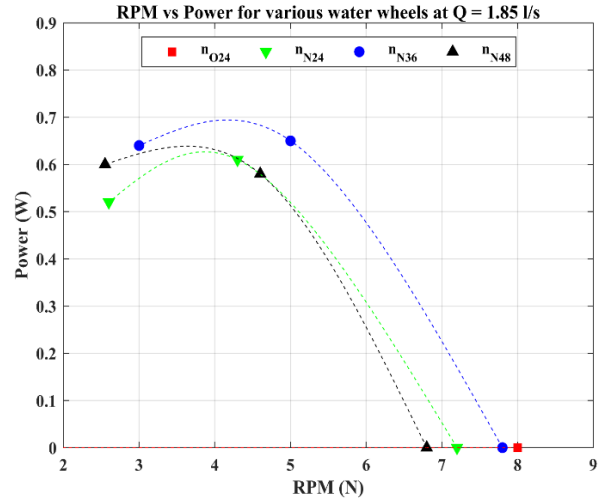

(a)

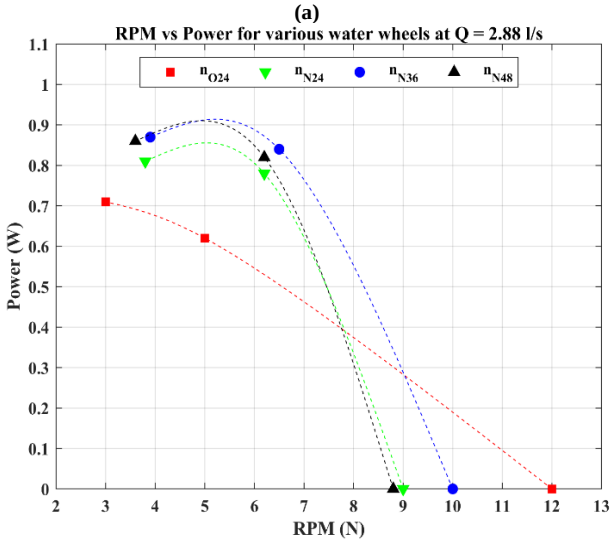

(b)

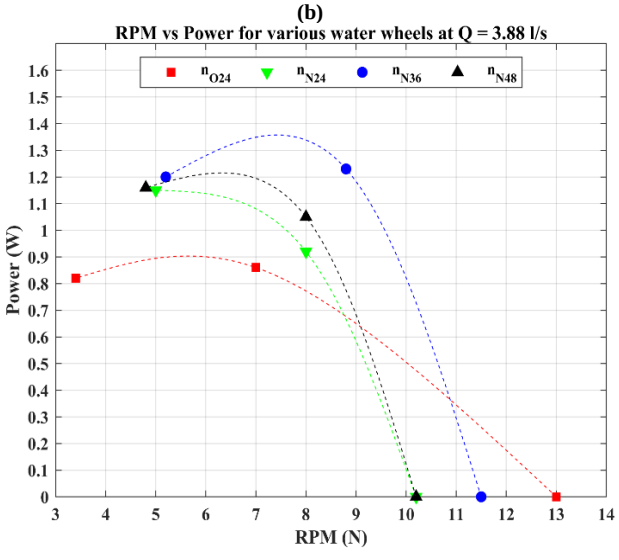

(c)

Fig. 7 Effect of blade design and count on Power output for varied flow rates of (a) Q=1.851 l/s, (b) Q=1=2.88 l/s and (c) Q=3.88 l/s undershot water wheel.

Figure 7 shows the power generated by nO24, nN24, nN36, and nN48 for different applied loads and the flowrates 1.85 L/s, 2.88 L/s, 3.88 L/s. The changed geometry of the blade to the curved shape has resulted in an increased maximum power output of up to 27% compared to the flat blade NO24 water wheel. Further, with the increase in blade count from 24 (nN24) to 36 (nN36), the power increased to 8.2% at 1.85 L/s, 5.3% at 2.88 L/s and 17.4% at 3.88 L/s. The nN36 water wheel produced maximum power output (1.35W) compared to nN24, nN36, and nN48. As the blade count increases from 36 (nN36) to 48 (nN48), a decline in power is observed, and the maximum power drop is 7% at 1.85 L/s and 11% at 3.88 L/s.

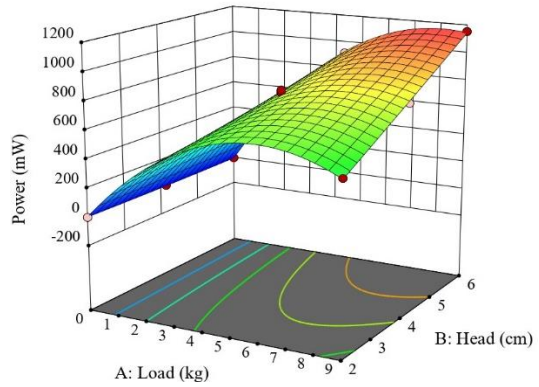

(a)

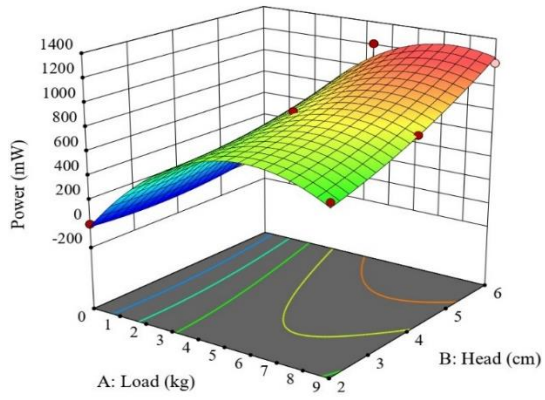

(b)

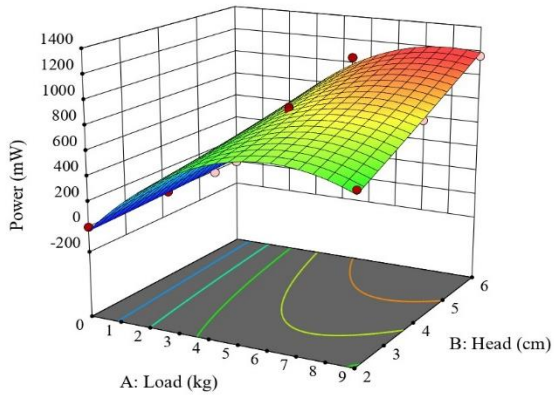

(c)

Fig. 8 Response curves generated for (a) nN24, (b) nN36, and (c) nN48 undershot water wheel.

Figure 8 illustrates the response curves for undershot water wheels with 24 (nN24), 36 (nN36), and 48 (nN48) blades, depicting the relationship between input conditions such as flow rates and applied loads and performance metrics like power output and efficiency. The response curve for nN24 shows almost a linear increase in power output, and an R^2 value of 0.99 shows an excellent fit, because there was hardly any obstructed flow.

The nN36 wheel produces the highest power output with the best efficiency in the medium flow rates. The efficiency dropped sharply at the higher flow rates while still producing power; the R^2 value of 0.87 shows the variance came from the increased blade count.

The nN48 wheel had a strong initial increase in power output but began to plateau at the higher flow rates where flow was obstructed by narrow blade spacing, and it seems to follow the trend with its R^2 value of 0.93. Altogether, the curves show that nN36 gives the best mix between efficiency and power output, while nN24 gives consistent results without really restricting flow nN48 shows the limitation of hydrodynamic drag and the turbulence effects in flow due to increased blade spacing.

4.1. Performance Limitations of the nO24 Water Wheel

The nO24 bi-fold flat blade water wheel design exhibited substantial performance limitations as applied loads increased. When the flow rate was 1.85 L/s, and an applied load of 9 kg was placed on the wheel, it was unable to turn and stalled completely. It appeared that this failure could be attributed to the reduced hydrodynamics efficiency of the bi-fold blade design that caused recirculation and turbulence between adjacent blades, which wasted energy rather than transferring momentum to the wheel.

Even at moderate loads of 4.5 kg, the wheel experienced a sharp decrease in torque and rotational stability, indicating the blade geometry was incapable of maintaining continuous energy transfer. Further contributing to the inefficiency of the nO24 design was the number of blades, which was much lower than the nN36 and nN48 wheel designs, and a reduced ability for contact surface with the flowing water resulted in insufficient torque to overcome applied resistance.

The completed experimental work highlighted that this nO24 wheel design was load sensitive, which prevented the wheel from being considered in any working scenario with load instability.

In contrast, the nN24, nN36, and nN48 curved-blade designs operated steadily, approximating the 4.5 and 9 kg applied load conditions, which relates to the optimized geometry and spacing of blades that improved the load capacity and, more importantly, the performance stability of the designs.

5. Conclusion

This study explored the impact of blade count and geometry on the performance of undershot water wheels, aiming to improve efficiency and power output for small-scale hydropower applications. Four configurations were tested under varied flow rates and loads to assess hydraulic and mechanical efficiency. Key insights and findings from the experiments are summarized below:

- The nO24 water wheel, featuring bi-fold blades, ceased functioning under higher loads at a low flow rate of 1.85 L/s, underscoring its design limitations.
- The curved-blade nN24 wheel achieved a maximum efficiency of 58% at 3.9 RPM, outperforming nO24 by 6% and 5% at flow rates of 2.88 L/s and 3.88 L/s, respectively.
- The nN36 water wheel demonstrated the highest efficiency (65% at 1.85 L/s) and the greatest power output (1.35 W) among all configurations tested.
- Increasing the blade count from 24 (nN24) to 36 (nN36) enhanced power output by up to 17.4% at the highest flow rate of 3.88 L/s.
- The nN48 wheel exhibited diminishing returns in efficiency and power due to flow blockage caused by narrow blade spacing, resulting in a power drop of 7% at 1.85 L/s and 11% at 3.88 L/s compared to the nN36 wheel.
- The R^2 values for nN24 (0.99), nN36 (0.87), and nN48 (0.93) confirmed the reliability of the experimental data and response curves.
- The curved-blade design proved more effective at harnessing kinetic energy, contributing to a 27% increase in maximum power compared to flat-blade designs.
- Optimization of blade count is critical for balancing efficiency and power, with 36 blades identified as the optimal configuration for the tested conditions.

These findings are novel and indicate that curved blades and optimized blade counts greatly improve the ability of undershot water wheels to produce power and are suitable as small-scale hydropower sources.

Future studies should look into blade counts between 36 and 48 using CFD and further experimental work. Realizing site-specific optimization, selecting pumps, and integration with energy storage could grow the application potential of water wheels for off-grid and remote energy applications.

These research findings have significant implications for small hydropower, rural electrification, and agricultural water lifting systems. The use of optimized curved-blade undershot wheels for electricity generation allows the use of low-head water resources to create dependable energy supplies for decentralized energy and mini-grids or produce electricity for stand-alone systems. The ability to produce higher torque to lift water from low-lying sources for agriculture has the

potential to increase agricultural productivity and food security in rural systems. Additionally, undershot wheels can be directly integrated into irrigation systems, providing a means for rural communities to produce electricity and water pumping while providing sustainable, low-cost approaches.

5.1. Future Scope

In addition to the immediate applications of this methodology, future research should elaborate on hybrid renewable systems that involve combining water wheels with solar or wind technologies, assess the potential ecological impacts of each developer or project to ensure biodiversity-sensitive deployment of water wheels, and compare and contrast the potential long-term performance of curved-blade undershot wheels.

Practically, curved-blade undershot types of wheels would be favoured by performance, efficiency, turbulence, and durability, when compared to flat-bladed designs, in terms of their long-term performance potential. Curved profiles effectively reduce cavitation and flow separation and reduce the susceptibility to fatigue and mechanical wear.

Systematic maintenance strategies include regular inspections, removing debris or biofouling, and replacing the high-stress components as a preventative measure to ensure reliable operation. This resumes with the selection of corrosion-resistant products such as stainless steel or composites to maximize operational performance.

Moreover, developing the watering system and real-time monitoring tools, such as IoT-based sensors to track torque and efficiency in real time, will help predict maintenance periods to maximize operational performance. When all three are implemented, undershot water wheels remain operational and sustainable over an extended period in real-world applications.

Nomenclature

Symbol	Description (with Unit)
A	Area (m^2)
C	Clearance from the bed (mm)
D	Depth of water from free surface (mm)
D_e	External diameter (mm)
d	Blade curvature diameter (mm)
d_s	Shaft diameter (mm)
H_w	Water head in (mm)
L	Load applied (kg)
l	Blade length (mm)
N	Number of blades (none)
P_h	Hydraulic power (W)
P_s	Shaft power (W)
Q	Water discharge (m^3/s)
r_s	Shaft radius (m)
T	Torque applied (Nm)
t	Torque collar thickness (mm)
V	Water velocity (m/s)
W	Width (mm)
α	Water inlet angle (degrees, °)
Δh	Manometer head difference (m)
ρ	Density (kg/m^3)
θ	Water inlet angle (degrees, °)
η_w	Efficiency of water wheel (%)
w	Related to water
b	Blade properties
p	Prototype values
s	Shaft properties
nO24	Original water wheel design with 24 blades
nN24	Curved blade water wheel with 24 blades
nN36	Curved blade water wheel with 36 blades
nN48	Curved blade water wheel with 48 blades
ANOVA	Analysis of Variance
CCD	Central Composite Design
CFD	Computational Fluid Dynamics
DOE	Design of experiments
PLA	Polylactic Acid (3-D Printing Material)
PIV	Particle image velocimetry
RPM	Revolutions Per Minute
R^2	Coefficient of Determination
3D	Three dimension

Funding Statement

This work received financial support from the Early Career Research Award, Science and Engineering Research Board, Department of Science and Technology, India, under grant no. ECR/2017/002945, as well as the support received under the UPES-SEED grant program from the University of Petroleum and Energy Studies."

Acknowledgments

The authors acknowledge the support from the Department of Mechanical Engineering and the R&D Department of UPES, Dehradun, India. We sincerely appreciate both departments' collaborative contributions to this research.

Prashanth Kumar S: Conceptualization, Data Curation, Investigation, writing – Original Draft, Visualization, Software; Ramesh Kumar Donga: Conceptualization, Data Curation, Software, Resources; Ashish Karn: Conceptualization, Resources, Writing - Review & Editing, Supervision, Funding acquisition, Formal analysis, Project administration."

References

[1] Alexandru Moldoveanu, and Daniela Popescu, "Assessment of Small Hydropower Potential by Software. Case Study," *Matec Web Conference: 21st Innovative Manufacturing Engineering & Energy International Conference*, vol. 112, pp. 1-6, 2017. [CrossRef] [Google Scholar] [Publisher Link]

[2] Yury Dementyev et al., "Gearless Micro Hydropower Plant for Small Water-Course," *Acta Polytechnica Hungarica*, vol. 14, no. 4, pp. 155-166, 2017. [CrossRef] [Google Scholar] [Publisher Link]

[3] Nor Fadilah Yah, Mat Sahat Idris, and Ahmed Nurye Oumer, "Numerical Investigation on Effect of Immersed Blade Depth on the Performance of Undershot Water Turbines," *Matec Web Conference: The 3rd International Conference on Mechanical Engineering Research*, vol. 74, pp. 1-5, 2016. [CrossRef] [Google Scholar] [Publisher Link]

[4] Emanuele Quaranta, *Innovative Projects and Technology Implementation in the Hydropower Sector*, Technological Innovations and Advances in Hydropower Engineering, IntechOpen, 2022. [CrossRef] [Google Scholar] [Publisher Link]

[5] Mehmet Bilgili, and Arif Ozbek, "An Overview of Micro-Hydropower Technologies and Design Characteristics of Waterwheel Systems," *Çukurova University Faculty of Engineering Journal*, vol. 31, no. 1, pp. 117-134, 2016. [CrossRef] [Google Scholar] [Publisher Link]

[6] Yasmina Martínez et al., "Impact of Small-Scale Hydropower Stations on Macroinvertebrate Communities for Regulated Rivers," *Limnetica*, vol. 39, no. 1, pp. 317-334, 2020. [CrossRef] [Google Scholar][Publisher Link]

[7] Emanuele Quaranta, and Gerald Müller, "Sagebien and Zuppinger Water Wheels for Very Low Head Hydropower Applications," *Journal of Hydraulic Research*, vol. 56, no. 4, pp. 526-536, 2018. [CrossRef] [Google Scholar] [Publisher Link]

[8] Muhammad Asim et al., "Design and Parametric Optimization of the High-Speed Pico Waterwheel for Rural Electrification of Pakistan," *Sustainability*, vol. 14, no. 11, pp. 1-22, 2022. [CrossRef] [Google Scholar] [Publisher Link]

[9] Suhartono Suhartono et al., "The Performances of Undershot Waterwheel with Butterfly-Shaped Blades and the Radius of Grasshopper's Elbow: The Utilization Efforts for River Electrical Energy Potential," *Jurnal Ilmiah Pendidikan Fisika Al-Biruni*, vol. 11, no. 1, pp. 1-17, 2022. [CrossRef] [Google Scholar] [Publisher Link]

[10] Yasuyuki Nishi et al., "Study on an Undershot Cross-Flow Water Turbine With Straight Blades," *International Journal of Rotating Machinery*, vol. 2015, pp. 1-10, 2015. [CrossRef] [Google Scholar] [Publisher Link]

[11] Piyawat Sritram, and Ratchaphon Suntivarakorn, "Comparative Study of Small Hydropower Turbine Efficiency at Low Head Water," *Energy Procedia*, vol. 138, pp. 646-650, 2017. [CrossRef] [Google Scholar] [Publisher Link]

[12] E.Y. Setyawan et al., "Design of Low Flow Undershot Type Water Turbine," *Journal of Science Applied Engineering*, vol. 2, no. 2, pp. 50-55, 2019. [CrossRef] [Google Scholar] [Publisher Link]

[13] Manh Hung Nguyen, Haechang Jeong, and Changjo Yang, "A Study on Flow Fields and Performance of Water Wheel Turbine Using Experimental and Numerical Analyses," *Science China Technological Sciences*, vol. 61, pp. 464-474, 2018. [CrossRef] [Google Scholar] [Publisher Link]

[14] Emanuele Quaranta, and Roberto Revelli, "Hydraulic Behavior and Performance of Breastshot Water Wheels for Different Numbers of Blades," *Journal of Hydraulic Engineering*, vol. 143, no. 1, pp. 1-10, 2017. [CrossRef] [Google Scholar] [Publisher Link]

[15] Luther Sule, Andi Amijoyo Mochtar, and Onny Sutresman, "Performance of Undershot Water Wheel with Bowl-shaped Blades Model, Performan," *International Journal of Technology*, vol. 11, no. 2, pp. 278-287, 2020. [CrossRef] [Google Scholar] [Publisher Link]

[16] Avita Ayu Permanasari et al., "Experimental Investigation and Optimization of Floating Blade Water Wheel Turbine Performance Using Taguchi Method and Analysis of Variance (ANOVA)," *IOP Conference Series: Materials Science and Engineering: International Conference on Condensed Matters and Advanced Materials*, Malang, Indonesia, vol. 515, pp. 1-11, 2019. [CrossRef] [Google Scholar] [Publisher Link]

[17] Wenjin Feng et al., "Experimental and Numerical Analysis of the Clearance Effects between Blades and Hub in a Water Wheel Used for Power Generation," *Water*, vol. 14, no. 22, pp. 1-20, 2022. [CrossRef] [Google Scholar] [Publisher Link]

[18] Emanuele Quaranta, and Roberto Revelli, "CFD Simulations to Optimize the Blade Design of Water Wheels," *Drinking Water Engineering and Science*, vol. 10, no. 1, pp. 27-32, 2017. [CrossRef] [Google Scholar] [Publisher Link]

[19] Mengshang Zhao et al., "Performance Investigation of the Immersed Depth Effects on a Water Wheel Using Experimental and Numerical Analyses," *Water*, vol. 12, no. 4, pp. 1-17, 2020, [CrossRef] [Google Scholar] [Publisher Link]

[20] Shakun Paudel et al., "Experimental and Numerical Study of Zuppinger Water Wheel Model," *Proceedings of the Institution of Civil Engineers - Water Management*, vol. 175, no. 4, pp. 206-216, 2022. [CrossRef] [Google Scholar] [Publisher Link]

[21] Emanuele Quaranta, and Gerald Müller, "Noise Generation and Acoustic Impact of Free Surface Hydropower Machines: Focus on Water Wheels and Emerging Challenges," *International Journal of Environmental Research and Public Health*, vol. 18, no. 24, pp. 1-7, 2021. [CrossRef] [Google Scholar] [Publisher Link]

[22] Dan Mugisidi et al., "Development of the Dethridge Wheel Blade Shape for Hydropower Generation in Irrigation Canals in Indonesia," *Journal of Advanced Research in Fluid Mechanics and Thermal Sciences*, vol. 98, no. 2, pp. 146-156, 2022. [CrossRef] [Google Scholar] [Publisher Link]

[23] Yasuyuki Nishi et al., "Study on Performance Improvement of an Axial Flow Hydraulic Turbine with a Collection Device," *International Journal of Fluid Machinery and Systems*, vol. 9, no. 1, pp. 47-55, 2016. [CrossRef] [Google Scholar] [Publisher Link]

[24] Irwan Lie Keng Wong et al., "Performance of Undershot Waterwheel Curved Blade of the Laboratory Scale," *Materials Science Forum*, vol. 967, pp. 250-255, 2019. [CrossRef] [Google Scholar] [Publisher Link]

[25] E. Quaranta, and R. Revelli, "Optimization of Breastshot Water Wheels Performance Using Different Inflow Configurations," *Renewable Energy*, vol. 97, pp. 243-251, 2016. [CrossRef] [Google Scholar] [Publisher Link]

[26] N.F. Yah et al., "Numerical Investigation on Effect of Blade Shape for Stream Water Wheel Performance," *IOP Conference Series: Materials Science and Engineering: International Conference on Innovative Technology, Engineering and Sciences*, Pekan Campus Library, Malaysia, vol. 342, pp. 1-11, 2018. [CrossRef] [Google Scholar] [Publisher Link]

[27] Piyawat Sritram, and Ratchaphon Suntivarakorn, "The Efficiency Comparison of Hydro Turbines for Micro Power Plant from Free Vortex," *Energies*, vol. 14, no. 23, pp. 1-13, 2021. [CrossRef] [Google Scholar] [Publisher Link]

[28] Rahmat Boli et al., "Analisis Daya Output Dan Efisiensi Kincir Air Sudu Miring Yang Bekerja Pada Saluran Horizontal," *Gorontalo Journal of Infrastructure & Science Engineering*, vol. 1, no. 2, pp. 1-36, 2018. [CrossRef] [Google Scholar] [Publisher Link]

[29] Abhishekkumar Shingala et al., "Genetic Optimisation of a Free-Stream Water Wheel Using 2D Computational Fluid Dynamics Simulations Points towards Design with Fully Immersed Blades," *Energies*, vol. 15, no. 10, pp. 1-20, 2022. [CrossRef] [Google Scholar] [Publisher Link]

[30] Raj Kumar Chaulagain, Akash Kalwar, and Purushottam Khatiwada, "Simulation and Experimental Analysis of Fixed and Rotating Blades on the Runner of Oryon Watermill Applicable for Head Drops of the Canal," *Advances in Mechanical Engineering*, vol. 16, no. 10, pp. 1-8, 2024. [CrossRef] [Google Scholar] [Publisher Link]

[31] Zelalem Girma, "Techno-Economic Feasibility of Small Scale Hydropower in Ethiopia: The Case of the Kulfo River, in Southern Ethiopia," *Journal of Renewable Energy*, vol. 2016, pp. 1-12, 2016. [CrossRef] [Google Scholar] [Publisher Link]

[32] Asral Asral, Musthafa Akbar, and Syafri Syafri, "The Performance of Undershot Water Turbine Combined With Spiral Tube Pump On Empowerment of Energy Resources Local Contiguous Small River," *Journal of Ocean, Mechanical and Aerospace -Science and Engineering*, vol. 42, no. 1, pp. 19-23, 2017. [CrossRef] [Google Scholar] [Publisher Link]

[33] Dewi Puspita Sari et al., "Blade Configuration and Depth Ratio Impact on Undershot Waterwheel in Compact Irrigation for Sustainable Off-Grid Electrification," *Journal of the Brazilian Society of Mechanical Sciences and Engineering*, vol. 47, 2025. [CrossRef] [Google Scholar] [Publisher Link]

[34] Miguel M. Uamusse et al., "Mini-Grid Hydropower for Rural Electrification in Mozambique: Meeting Local Needs with Supply in a Nexus Approach," *Water*, vol. 11, no. 2, pp. 1-19, 2019. [CrossRef] [Google Scholar] [Publisher Link]

[35] Ahmad Firdaus Abdul Jalil, Jagadeesh Pasupuleti, and M. Reyasudin Basir Khan, "Feasibility Evaluation of Micro-Hydropower System Generation for Different Types of Sewage Treatment Plants," *International Journal of Recent Technology and Engineering*, vol. 8, no. 4, pp. 6338-6341, 2019. [CrossRef] [Google Scholar] [Publisher Link]

[36] Jose Bernardes et al., "Hydropower Operation Optimization Using Machine Learning: A Systematic Review," *AI*, vol. 3, no. 1, pp. 78-99, 2022. [CrossRef] [Google Scholar] [Publisher Link]

[37] Christine Ann Teodoro, "Harnessing Hydroelectric Energy from Water Irrigation Pumps: A Sustainable Lighting Solution for Agricultural Fields and Fishponds," *E3S Web of Conferences: 1st International Conference on Advanced Materials & Sustainable Energy Technologies*, vol. 488, pp. 1-24, 2024. [CrossRef] [Google Scholar] [Publisher Link]

[38] Nerantzis Kazakis et al., "Groundwater Depletion. Are Environmentally Friendly Energy Recharge Dams a Solution?," *Water*, vol. 16, no. 11, pp. 1-20, 2024. [CrossRef] [Google Scholar] [Publisher Link]

[39] G. Müller, and C. Wolter, "The Breastshot Waterwheel: Design and Model Tests," *Proceedings of the Institution of Civil Engineers - Engineering Sustainability*, vol. 157, no. 4, pp. 203-211, 2004. [CrossRef] [Google Scholar] [Publisher Link]

[40] Bruna A. Da Silva, Renata E. De Oliveira, and Tomas F. Domingues, "Multifunctionality, Social Benefits, and Engagement: Insights for Forest Restoration Success from a Study Case in Brazil," *Restoration Ecology*, vol. 33, no. 1, 2025. [CrossRef] [Google Scholar] [Publisher Link]

[41] Nicola Favretto et al., "Knowledge Exchange Enhances Engagement in Ecological Restoration and Rehabilitation Initiatives," *Restoration Ecology*, vol. 30, no. 2, pp. 1-8, 2021. [CrossRef] [Google Scholar] [Publisher Link]

[42] Emanuele Quaranta, Jean Pierre Perrier, and Roberto Revelli, "Optimal Design Process of Crossflow Banki Turbines: Literature Review and Novel Expeditious Equations," *Ocean Engineering*, vol. 257, pp. 1-15, 2022. [CrossRef] [Google Scholar] [Publisher Link]

[43] Dilshod Kodirov, and Obid Tursunov, "Calculation of Water Wheel Design Parameters for Micro Hydroelectric Power Station," *Conferences: XXII International Scientific Conference "Construction the Formation of Living Environment,"* vol. 97, pp. 1-11, 2019. [CrossRef] [Google Scholar] [Publisher Link]

[44] Susan E. Kelly, and Lawrence C. Murdoch, "Measuring the Hydraulic Conductivity of Shallow Submerged Sediments," *Ground Water*, vol. 41, no. 4, pp. 431-439, 2003. [CrossRef] [Google Scholar] [Publisher Link]

[45] A.J. Archer, and R. Evans, "Dynamical Density Functional Theory and Its Application to Spinodal Decomposition," *The Journal of Chemical Physics*, vol. 121, no. 9, pp. 4246-4254, 2004. [CrossRef] [Google Scholar] [Publisher Link]

[46] Tineke Saroinsong et al., "Performance of Three-Bladed Archimedes Screw Turbine," *ARPN Journal of Engineering and Applied Sciences*, vol. 11, no. 15, pp. 9491-9495, 2016. [Publisher Link]